

Revision 1 - Word count: 8101

Radiation-Induced Changes in Vanadium Speciation in Basaltic Glasses: Implications for Oxybarometry Measurements Using Vanadium K-edge X-ray Absorption Spectroscopy

ANTONIO LANZIROTTI^{1,*}, STEPHEN SUTTON^{1,2}, MATTHEW NEWVILLE¹, AND ELISABET HEAD³

¹ Center for Advanced Radiation Sources, The University of Chicago, Argonne, IL 60439, USA

² Department of the Geophysical Sources, The University of Chicago, Argonne, IL 60439, USA

³ Department of Earth Science, Northeastern Illinois University, Chicago, IL 60625, USA

ABSTRACT

Magmatic oxygen fugacity (fO_2) exerts a primary control on the discrete vanadium (V) valence states that will exist in quenched melts. Vanadium valence proxies for fO_2 , measured using X-ray absorption near-edge spectroscopy (XANES), can provide highly sensitive determinations of the redox conditions in basaltic melts. However, X-ray beam-induced changes in V speciation will introduce uncertainty in the calculated average V valence (V^*) that must be properly evaluated in order to make meaningful interpretations of the igneous evolution of the system. The study presented here showed that beam-induced modifications in V speciation are observed in silicate glasses that are dependent on the radiation dose rate used during analysis. Changes in V speciation are observed to be most pronounced at the highest flux density tested, 9.25×10^{11} ph/s/ μm^2 (photons per second per square micrometer), with rapid changes occurring in the first 200s of analysis. The high dose rate conditions result in changes in calculated $V^* \sim 0.3$ valence unit for the most oxidized glass analyzed ($V^* = 4.94$), which can correspond to ~ 0.5 log unit reduction in calculated fO_2 . However, at flux densities $\leq 1.13 \times 10^9$ ph/s/ μm^2 , measured changes in V^* were found to be < 0.03 for all standard glasses analyzed. The degree of reduction observed during analysis is also found to be progressively smaller as the initial V^* of the glass

25 decreases, such that magmatic glasses with V^* values ≤ 3.7 show no statistically-significant
26 change in calculated valence during analysis at any flux density tested. For most terrestrial
27 magmatic glasses, where V^* is found to be < 4 , beam induced changes in V^* can be effectively
28 minimized (< 0.04), within analytical uncertainty of the XAFS analysis, by limiting flux
29 densities to be $\leq 1 \times 10^9$ ph/s/ μm^2 .

30 INTRODUCTION

31 Accurate estimates of the intrinsic oxygen fugacity ($f\text{O}_2$) of magmas are important for
32 constraining source composition and understanding the conditions under which melts are
33 generated, their sub-liquidus evolution and crystallization history, and the composition and
34 evolution of volcanic gases released to the atmosphere (Sato 1978; Mathez 1984; Christie et al.
35 1986; Ballhaus et al. 1990; Carmichael 1991; Kelley and Cottrell 2009). Oxybarometers of
36 varying types provide geologists analytical approaches for indirectly constraining magmatic $f\text{O}_2$
37 through chemical analysis of varying primary igneous phases. Of the approaches currently
38 available for oxybarometry, those based on X-ray absorption fine structure (XAFS) spectroscopy
39 (Sutton et al. 2005, 2005, 2020; Cottrell et al. 2009; Bunker 2010; Jugo et al. 2010; Henderson et
40 al. 2014; Trail et al. 2015; Lanzirotti et al. 2018) are particularly attractive due to the high
41 sensitivity of XAFS in detecting subtle changes in the chemical speciation of redox-sensitive
42 elements in igneous minerals and/or glasses in response to changing magmatic $f\text{O}_2$. Various
43 XAFS oxybarometers have been developed for magmatic systems, including those based on
44 measuring changes in chemical speciation of multivalent elements such as Fe, S, Ti, Mn, Cr, Eu,
45 Ce and V (reviewed in Sutton et al. 2020 and references therein). Vanadium XAFS
46 oxybarometry has broad applicability to terrestrial and extraterrestrial igneous materials since its
47 valence varies continuously from V^{3+} to V^{5+} over a wide range of $f\text{O}_2$ (Giuli et al. 2004; Sutton et

48 al. 2005; Karner et al. 2006; Lanzirotti et al. 2018; Nakada et al. 2020). In terrestrial basaltic
49 melts, the $V^{3+} \leftrightarrow V^{4+}$ and $V^{4+} \leftrightarrow V^{5+}$ multivalent couples span an oxygen fugacity range relative
50 to the nickel-nickel oxide (NNO) buffer from about NNO-6 to NNO+3.5 (Papike et al. 2005).

51 An analytical complication in the application of XAFS oxybarometers with respect to
52 mineral and glass analysis is the potential for inducing changes in the valence and/or crystal-
53 chemical environment of the element of interest due to exposure of samples to the synchrotron
54 X-ray beam. Such phenomena have been documented in several systems and have been found to
55 be particularly pronounced for hydrous magmatic glasses. For example, sulfur valence state
56 changes have been observed during XAFS analysis of volcanic glasses and melt inclusions
57 (Rowe et al. 2007; Wilke et al. 2008; Klimm et al. 2012); most commonly reported is the
58 generation of S^{4+} species in glasses, generally attributed to reduction of S^{6+} during irradiation
59 (Wilke et al. 2008). In another example, Cottrell et al. (2018) showed that Fe^{2+} in hydrous
60 silicate glasses can undergo rapid oxidation upon exposure to radiation. In the most hydrous
61 basaltic glasses they analyzed, they showed that radiation-induced increase in $Fe^{3+}/\Sigma Fe$ ratio of
62 up to 0.16 can be observed after several minutes of irradiation at X-ray flux densities of $\sim 2 \times 10^9$
63 $ph/s/\mu m^2$. They also showed that for Fe, the rate of oxidation also correlates with the product of
64 water concentration and ferrous/ferric iron oxide ratio in the glass. Interestingly, in anhydrous
65 glasses, they observed no statistically significant change in Fe valence under any beam
66 conditions, which led them to infer that it is radiation-induced hydrolysis which may drive
67 oxidation of Fe^{2+} in these magmatic glasses. Other studies have noted that anhydrous silicate
68 glasses with high concentrations of Fe often do not show evidence of beam-induced changes in
69 Fe valence (Camara and Oel 1984). However, in soda-lime silicate glasses where Fe is doped at
70 trace element concentrations (150-5000 ppm), Fe^{3+} has been shown to undergo X-ray induced

71 reduction (Camara and Oel 1984; Gonçalves Ferreira et al. 2013). Such reduction was
72 hypothesized to result from the production of localized defects within the glass matrix during
73 irradiation, where electron-hole pairs associated with the defect sites act to change the valences
74 of incorporated trace Fe. We hypothesize that other multi-valent trace elements in natural silicate
75 glasses, such as V, may display similar behavior on irradiation.

76 This study presents new observations regarding X-ray beam-induced changes in V valence in
77 silicate glasses. Although the potential for radiation-induced changes in V valence in the analysis
78 of natural silicate glasses has been alluded to in published studies (Lanzirotti et al. 2018), we are
79 unaware of any systematic study that has sought to describe and quantify the magnitude of any
80 observed changes with radiation dose rate that are relevant to geochemical studies. For V XAFS
81 oxybarometry to provide accurate and precise estimates of changing oxygen fugacity in
82 magmatic systems, it is important to understand and quantify how irradiation during XAFS
83 analysis can modify the spectral features used to calculate the average V valence of igneous
84 systems.

85 **SAMPLES AND ANALYTICAL PROCEDURES**

86 Four synthetic glasses and two natural volcanic glasses were analyzed by V K-edge XAFS at
87 varying incident flux densities. The synthetic samples are from a suite of anhydrous forsterite-
88 anorthite-diopside (FAD) composition glasses doped to provide V concentrations of ~ 3000 ppm.
89 This suite of glasses were synthesized at 1 atm pressure, at equilibration temperatures of 1310 -
90 1320°C and at $\log fO_2$ ranging from -15.5 to -4.55. Their synthesis is fully described in Hanson
91 and Jones (1998). For this study, four glasses in the suite were evaluated for radiation-induced
92 changes in V valence, chosen because they were equilibrated over a broad range of ~7 log units
93 fO_2 , (expressed here relative to nickel-nickel oxide buffer, NNO, Huebner and Sato, 1970):

94 FAD_V2a ($\log fO_2$ -11.6, ΔNNO -5.3), FAD_V4 ($\log fO_2$ -9.6, ΔNNO -3.3), FAD_V1a ($\log fO_2$ -
95 7.1, ΔNNO -0.7) and FAD_V3 ($\log fO_2$ -4.6, ΔNNO +1.7). The two natural glasses studied are
96 Smithsonian Institution NMNH National Rock Collection samples (Jarosewich et al. 1980)
97 designated A-99 (NMNH 113498-1), a sample of fresh basaltic glass collected from the
98 Makaopuhi Lava Lake, Hawaii, and VG-2 (NMNH 111240-52), a sample of fresh basaltic glass
99 dredged from the Juan de Fuca Ridge. Published estimates for NNO-relative fO_2 for A-99 and
100 VG-2, based on V XAFS oxybarometry, were ΔNNO -1.28 and ΔNNO -0.08 respectively
101 (Lanzirotti et al. 2018). Absolute vanadium abundances have not been reported for these two
102 glasses, but natural basaltic glasses generally have V concentrations between ~200–400 ppm,
103 which is consistent with the X-ray fluorescence intensities measured for V K emission lines. All
104 samples were prepared as polished (using 0.5 micron diamond-embedded polishing paper),
105 epoxy embedded chips where the glass thickness was large compared to the sampling depth of V
106 K-edge X-rays. Previous V K-edge XAFS analyses of these samples are described in Lanzirotti
107 et al. (2018), Sutton et al. (2005) and Karner et al. (2006).

108 Vanadium K-edge XAFS spectra were measured using the 13-ID-E undulator-based
109 microprobe at the GeoSoilEnviro-CARS sector, Advanced Photon Source (APS), Argonne
110 National Laboratory, USA. The optical and instrumental configuration of the beamline are
111 described in Lanzirotti et al. (2016, 2018) and (Sutton et al. 2017). Monochromatic radiation was
112 provided by a cryogenically-cooled, double-crystal monochromator using a Si(111)
113 monochromator crystal set. Beam focusing to the sample is provided by a pair of 240 mm long,
114 highly polished, dynamically-bent bare silicon mirrors in a Kirkpatrick-Baez (KB) geometry
115 capable of generating focused spot sizes of $\sim 1 \times 2 \mu\text{m}$ (FWHM) and of providing incident
116 monochromatic flux (I_0) in excess of 5×10^{12} ph/s, which is measured in a helium-filled, 200 mm-

117 long ion chamber just upstream of the KB mirror optics. For the experiments described here, X-
118 ray flux density delivered to the sample was controlled by dynamic defocusing of the beam,
119 using the KB optics, and by filtering of the incident beam, using high-purity aluminum filters.
120 For consistency with previous published data from the beamline, the sample-impinging flux
121 densities that are reported here are calculated based on measured I_0 , which is monitored upstream
122 of the mirror focusing optics. Flux is calculated using measured current in the 200 mm long ion
123 chamber, assuming 100% He gas at atmospheric pressure and effective ionization potential for
124 He from Knoll (2010). The KB mirrors have reflection efficiencies of ~80%, so flux delivered to
125 the samples is estimated to be 60% of the measured I_0 flux. The energy of the first derivative
126 peak of V metal foil provided a V K-edge energy of 5463.76 eV, consistent with value
127 determined by Kraft et al. (1996). Fluorescence spectra were collected using a Vortex ME4 and
128 Canberra SX7 silicon-drift diode detector arrays coupled to a high-speed digital spectrometer
129 system (Quantum Xpress3).

130 Full V K-edge XAFS spectra were collected at variable flux densities, 2.56×10^8 , 7.75×10^8 ,
131 6.25×10^{11} , and 9.25×10^{11} ph/s/ μm^2 , with each analysis conducted on a fresh sample spot. This
132 allowed us to compare the final shape of the XAFS spectra with increasing radiation dose and
133 evaluate any potential trends in changing V speciation over time. The XAFS spectra collected at
134 flux densities of 2.56×10^8 and 9.25×10^{11} ph/s/ μm^2 scanned the incident beam from 5365-5455
135 eV in 2.5 eV steps, from 5455-5490 eV in 0.15 eV steps, and from 5490-5645 eV in 2.0 eV steps
136 at 1 s per energy point. This allowed us to compare spectra with optimal signal/noise at the
137 highest and lowest flux densities tested, with one spectrum being collected in ~6 minutes (Fig.
138 1). More rapid XAFS spectra were also collected at flux densities of 7.75×10^8 and 6.25×10^{11}
139 ph/s/ μm^2 , scanning the incident beam from 5420-5455 eV in 3.5 eV steps, from 5455-5475 eV in

140 0.15 eV steps, from 5475-5500 eV in 2.5 eV steps and from 5500-5700 eV in 5.0 eV steps at 0.5
141 s per energy point. This allowed us to evaluate changes in spectral shape more quickly at two
142 flux densities that differ by a factor of ~800, with slightly poorer signal/noise, but with one
143 spectrum being collected in only ~1.5 minutes (Figs. 2, 3 and 4).

144 V^* values were calculated using the Sutton et al. (2005) calibration, derived from XAFS
145 spectra measured in synthetic glass standards produced under known fO_2 and temperature
146 conditions. Following the Sutton et al. protocol, each XAFS spectrum is first normalized to the
147 count rate measured at 5600 eV. The pre-edge peak intensity (I) is then measured as the
148 maximum intensity of the net pre-edge peak multiplet after normalized intensities are multiplied
149 by 1000 and after subtracting the edge step contribution. The effective vanadium valence, V^* is
150 then calculated as:

$$I = -153 + 199(V^*) - 106(V^*)^2 + 22.4(V^*)^3 \quad (1)$$

151 Tests were also conducted to constrain rates of reduction in glasses showing evidence of
152 decreases in V^* as a function of radiation dose rate using four flux densities covering more than
153 4 orders of magnitude: 1.69×10^6 , 1.38×10^8 , 1.13×10^9 , and 9.25×10^{10} ph/s/ μm^2 . A protocol
154 similar to that described by Cottrell et al. (2018) for evaluating beam-induced changes in Fe
155 valence was used for this purpose. For evaluating beam-induced changes in Fe valence in silicate
156 glasses Cottrell et al. measured the change in the peak amplitude of the second multiplet pre-
157 edge peak of the Fe K-edge with time at differing flux densities. Here, we evaluated the time
158 dependence of the measured V spectral intensity at an energy of 5468.15 eV, which sits on the
159 pre-edge peak, as a function of flux density (i.e., dose-rate). Each time series consists of
160 measurements at 1s intervals over 1500s of total irradiation and with each curve measured at a
161 fresh spot on the sample that had not been previously irradiated. The 13-ID-E monochromator

162 has been demonstrated (Sutton et al. 2017) to have no significant energy drift (<0.05 eV) as a
163 function of time, so that it is unlikely that any intensity changes measured are affected by energy
164 drift. Although pre-edge peak energies also increase with increasing valence, the energy shifts
165 are small (~ 1 eV from V^{3+} to V^{5+} , Sutton et al. 2005). Thus, although we are solely monitoring
166 changing intensity of the pre-edge peak at an energy of 5468.15 eV in constructing the rate-of-
167 change curves, this is the most convenient method for evaluating *potential* changes in valence at
168 very short accumulation times of 1 s. Thus, for the purposes stated here, the uncertainties
169 introduced by collecting intensities at a single energy are likely to be negligible.

170 RESULTS

171 *Observed Spectroscopic Changes Following Irradiation*

172 In V K-edge XAFS spectroscopy, increases in V valence are generally indicated by increases
173 in the net, normalized intensity of the pre-edge peak and shifting of the main absorption edge to
174 higher energy, although other changes in spectral shape are also noted (Wong et al. 1984; Sutton
175 et al. 2005; Lanzirrotti et al. 2018). The pre-edge peak results from the dipole forbidden $1s \rightarrow 3d$
176 transition and is coupled to metal-ligand symmetry; V species in regular octahedral coordination
177 with the O^{2-} ligand have the smallest observable pre-edge intensity while species in tetrahedral
178 coordination have the largest intensity. In glasses, these changes in coordination are coupled to
179 changes in V valence. Figure 1 shows edge-step normalized V K-edge XAFS spectra collected
180 for FAD_V3, the most oxidized glass analyzed, and FAD_V2a, the most reduced glass analyzed,
181 measured at flux densities of 2.56×10^8 (in red) and 9.25×10^{11} (in blue) $\text{ph/s}/\mu\text{m}^2$. In oxidized
182 glass FAD_V3, a decrease in the energy of the main absorption edge (E_0) of -1.1 eV and a
183 decrease in normalized, pre-edge peak intensity of -0.26 is observed (i.e., 26% decrease of the
184 above edge normalization level). These spectral changes and the observed changes in intensity

185 and energy of spectral resonances in the main absorption peak, the “white line,” are consistent
186 with reduction in V valence (Lanzirotti et al. 2018) as the radiation dose rate increases. Reduced
187 glass FAD_V2a displays a roughly similar decrease in E_0 of - 0.8 eV, but a small increase in pre-
188 edge peak intensity is also observed with increasing dose rate if the spectroscopic background is
189 not subtracted from the pre-edge peak. The inset plots in Fig. 1 show the relative magnitude of
190 the measured pre-edge peaks for both glasses after subtracting the edge step contribution via
191 spline fitting of the rising absorption edge. Although the background subtracted spectra for
192 oxidized glass FAD_V3 indicate an ~30% reduction in pre-edge peak intensity after subtraction
193 of the spectral background, the background subtracted peak intensities for reduced glass
194 FAD_V2a displays a <1% difference at the two flux densities tested.

195 Both the reduced and oxidized glass display increases in the intensity of a spectroscopic low
196 energy shoulder at ~ 5475 eV with increasing dose-rate. This feature sits on the rising absorption
197 edge just above the pre-edge peak (Fig. 1, dashed line). The increasing intensity of this shoulder
198 at ~5475 eV has the potential for elevating the pre-edge peak baseline, an effect that is more
199 significant in highly reduced glasses where the pre-edge peak intensities are small. In V XAFS,
200 the spectral shoulder that is observed on the rising absorption edge has been attributed to a
201 $1s \rightarrow 4p$ shakedown transition (Wong et al. 1984) and these features are thought to be associated
202 with charge transfer from the ligand to the metal. Thus observed changes in the absolute intensity
203 of these shoulder peaks potentially indicate that changes in vanadium-oxygen complexing are
204 occurring in these glasses with increasing radiation dose-rate.

205 To better evaluate the rate at which any observed spectroscopic changes occur, a series of
206 more rapid XAFS analyses were conducted at both low (7.75×10^8 ph/s/ μm^2) and high (6.25
207 $\times 10^{11}$ ph/s/ μm^2) flux density. Results of these analyses are shown in Fig. 2 for the reduced

208 synthetic glasses (FAD_V2a and FAD_V4), Fig. 3 for the oxidized synthetic glasses (FAD_V1a
209 ad FAD_V3) and in Fig. 4 for natural MORB glass VG-2. Shown are a series of 10 edge-step
210 normalized V K-edge XAFS spectra that were measured sequentially, with each scan acquired in
211 ~1.5 minutes, collected at low (left) and high (right) flux density. Acquisition of 10 total spectra
212 requires the glass to undergo irradiation at each flux density for a total time of ~15 minutes. The
213 inset plots on each figure show the pre-edge peak portion of each scan and provide calculated V^*
214 for each scan using the Sutton et al. (2005) calibration, which subtracts the pre-edge background.
215 We estimate that the uncertainty in calculated V^* from fitting the pre-edge peak intensity for any
216 individual scan under the conditions used is ~ 1.5% (1σ error, which is what is reported for
217 uncertainties below).

218 Observed trends in these spectra are consistent with those from Fig. 1. The most reduced
219 glass analyzed, FAD_V2a ($\log fO_2$ -11.6), gives a calculated mean V^* of $V^* 3.13 (\pm 0.01)$ at low
220 flux density and $V^* 3.10 (\pm 0.03)$ at high flux density (Fig. 2, top). Fig. 5 shows how the relative
221 calculated V^* for this series of analyses changes with time. For FAD_V2a, the first two spectra
222 collected at the high flux condition yield slightly more reduced V^* , but these are still within error
223 of the calculated mean for all 10 spectra in the series. Glass FAD_V4 ($\log fO_2$ -9.6), which was
224 equilibrated under slightly more oxidizing conditions, gives a calculated mean V^* of $3.62 (\pm$
225 $0.01)$ at low flux density and $V^* 3.47 (\pm 0.01)$ at high flux density (Fig. 2, bottom). After 200
226 seconds of irradiation, the FAD_V4 high flux sequence yields V^* values that are clearly more
227 reduced than what is measured at low flux, outside of the fitting uncertainties (Fig. 5).

228 In more oxidized glasses, this difference is accentuated with increasing valence. FAD_V1a
229 ($\log fO_2$ -7.1) gives a calculated mean V^* of $4.30 (\pm 0.01)$ at low flux density and $V^* 4.02 (\pm$
230 $0.03)$ at high flux density (Fig. 3, top). FAD_V3 ($\log fO_2$ -4.6) gives a calculated mean V^* of

231 4.94 (\pm 0.01) at low flux density and V^* 4.65 (\pm 0.08) at high flux density (Fig. 3, bottom). For
232 these glasses, all the high flux analyses are statistically distinct from what is measured at low
233 flux at all measured time points (Fig. 5). Natural MORB glass VG-2 provides calculated mean
234 V^* of 4.33 (\pm 0.03) when measured at low flux density and 4.14 (\pm 0.05) at high flux density,
235 very similar to results given by synthetic glass FAD_V1a, although uncertainties are slightly
236 higher due to the lower V abundance in MORB glass.

237 Other studies have also utilized time series measurements of pre-edge intensities measured
238 rapidly at a single energy to help evaluate rates of speciation changes for multi-valent elements
239 in silicate glasses as a function of flux density (Cottrell et al. 2018; Moussallam et al. 2019;
240 Gaborieau et al. 2020). By monitoring intensity changes at a single incident energy, rapid
241 changes that occur at the onset of X-ray exposure can be evaluated. Figure 6 shows such time
242 series analyses for the two most oxidized synthetic glasses analyzed (Fig. 6 top) and for the two
243 natural basaltic glasses (Fig. 6 bottom). Changing spectral intensities of the V pre-edge were
244 monitored at an incident energy of 5468.15 eV for four different flux densities (described above).
245 Accumulated counts were collected at 1s intervals over 1500s of total irradiation, and then
246 plotted as the relative fractional change in measured change intensity over time. It should be
247 noted, however, that although such time series can be used to monitor changes at very short time
248 intervals, such analyses can have large associated uncertainties due to low signal/noise
249 (particularly when absorber concentrations are low) and can be difficult to accurately correlate to
250 valence (V^*) due to an inability to evaluate potential changes in pre-edge spectral background.

251 At the highest flux density tested for these time series, $9.25e^{10}$ ph/s/ μm^2 , the two oxidized
252 synthetic glasses again show clear decreases in V pre-edge peak intensities with increasing
253 accumulated dose. An intensity change of \sim -11% is noted for FAD_V1a and -18% for FAD_V3

254 after 1500s of irradiation (Fig. 6 top). These are consistent with the full XAFS results. Although
255 the full XAFS scans were collected using up to a factor of 10 higher flux density, the shorter
256 accumulation time used in collecting the time series means that roughly similar levels of total
257 photons were delivered to the analysis point. The time series measurements, however, more
258 clearly show that the decreases in measured intensity changes at the pre-edge energy are non-
259 linear with continued irradiation. The curves measured for both glasses flatten over time,
260 suggesting they may have reached an equilibrium condition after 400s of exposure at the highest
261 flux densities tested. Natural basaltic glasses VG-2 and A-99 both show small decreases in count
262 rates at the pre-edge at the highest tested flux density of $\sim -5\%$. However, at the lower tested flux
263 densities, intensity changes are difficult to discern in these natural glasses within the analytical
264 uncertainty of measuring V $K\alpha$ fluorescence at the short 1s integration times used.

265 **DISCUSSION**

266 *Evaluating Potential Changes in Vanadium Valence During XAFS Analysis*

267 We used the empirically-derived formula of Sutton et al. (2005) to evaluate the potential
268 impact of the observed beam-induced changes in V speciation on the calculated average V
269 valence (V^*) of the glasses studied. The Sutton calibration calculates V^* on the basis of
270 measured, edge-step normalized, pre-edge peak intensities after subtraction of the rising edge
271 background. For V XAFS oxybarometric studies, the pre-edge peak intensity is found to have
272 high valence sensitivity, although it is important to recognize that changes in V coordination
273 within the glass network will also alter pre-edge peak intensities. The study by Sutton et al.
274 (2005) shows that in silicate glasses changes in the V pre-edge peak intensity changes are
275 predominately due to valence changes; the intensities for V^{4+} are about the same in VI and V
276 coordination and V^{5+} is about the same in IV and V. However, lower coordination numbers tend

277 to provide slightly more intense pre-edge peak intensities, so although the intensity changes are
278 dominated by changes valence, the magnitudes of valence effects reported here will be
279 overestimates if some of the observed intensity changes are also due to coordination changes.

280 It is clear from these analyses that V in silicate glasses will undergo measurable beam-
281 induced reduction at high flux densities when the average V valence in the glass, V^* , is greater
282 than ~ 3.7 . The degree of reduction is also observed to increase with increasing V^* of the glass.
283 The rapid XAFS measurements of the most oxidized glass analyzed, FAD_V3 (Fig. 3), gives a
284 mean V^* of 4.94 when measured at a low dose condition of 7.75×10^8 ph/s/ μm^2 and 4.65 at a
285 high dose condition of 6.25×10^{11} ph/s/ μm^2 . Therefore, an observed reduction in calculated V
286 valence (ΔV^*) of -0.3 when the flux density is increased by a factor of ~ 800 . With decreasing V^*
287 in the glass, the degree of observed reduction as a function of flux density at these conditions is
288 also observed to be smaller. In FAD_V1a the change in mean V^* similar, from 4.30 to 4.02
289 ($\Delta V^*=0.28$), in FAD_V4 from 3.62 to 3.47 ($\Delta V^*=0.15$), and in FAD_V2a from 3.13 to 3.10
290 ($\Delta V^*=0.03$). The results of both rapid XAFS scanning (Figs. 3 and 5) and from time series
291 analyses at the pre-edge peak (Fig. 6) also show that at flux densities at or below 7.75×10^8
292 ph/s/ μm^2 , changes in V^* are not statistically discernable over 1500s of irradiation. Extrapolation
293 of the observed trends suggests that glasses with starting V^* values near ~ 3.7 will display only
294 minimal change in pre-edge peak intensity with increasing dose.

295 Highly reduced glasses with calculated V^* less than 3.7 also likely undergo changes in V
296 speciation with irradiation. This is reflected by measured changes in overall spectral shape, shifts
297 in the energy of the rising absorption edge and changes in the intensity of the spectral
298 background near the pre-edge peaks. However, it remains unclear in these samples to what
299 degree these changes in speciation also involve changes in valence state. For the most reduced

300 glass analyzed, FAD_V2a, it was noted that calculated mean V^* only changes from 3.13 to 3.10
301 ($\Delta V^*=0.03$), arguably within statistical uncertainty. We also noted from the rapid XAFS analysis
302 (Figs. 2 and 5) that the first two spectra in this series, collected at the high flux condition, yield
303 slightly more reduced V^* , but still within error of the calculated mean for all 10 spectra in the
304 series. Thus some degree of beam-induced oxidation (as opposed to reduction) in these highly
305 reduced glasses cannot be discounted. However, the impact on calculated average valence
306 appears small.

307 In the natural basaltic glasses studied the degree of reduction observed appears comparable to
308 what is observed in the synthetic FAD glasses. In MORB glass VG-2 the mean V^* decreases
309 from 4.33 to 4.14 ($\Delta V^*=0.19$), very similar to what is observed in FAD_V1a, which yields a
310 generally similar mean V^* . Observed trends are proportionally similar for both synthetic and
311 natural glasses even though there are large differences in Fe concentration in the glasses
312 analyzed, which is significant in that it suggests that differences in Fe concentration have little
313 impact on the observed effect. Although Fe is present at only trace element concentrations in the
314 FAD glasses analyzed here (Lanzirotti et al. 2018), in natural basaltic glasses Fe concentrations
315 typically exceed 10 wt% and will be the most abundant multi-valent element present. It is worth
316 noting, however, that it is unknown if the degree or direction of beam-induced changes in V
317 valence in silicate glasses are impacted by the water content of the glass. All the glasses analyzed
318 here are relatively anhydrous, including the natural glasses. In studies of Fe valence in natural
319 glasses there is a clear correlation between water content and increasing degrees of Fe oxidation
320 with increasing flux density (Cottrell et al. 2018),

321 ***Discussion of Potential Mechanisms for Beam-Induce Changes in V Valence***

322 Studies examining the structural and chemical changes that occur in glasses exposed to
323 ionizing radiation have shown that irradiation can generate free electrons and holes which can
324 then be trapped in defect sites (Bishay 1970). These electron-hole pairs can act to change the
325 valences of incorporated trace elements spatially correlated with such defects (Camara and Oel
326 1984; El Batal and Naf 2005; Zhang et al. 2007; Abdelghany and ElBatal 2012; Gonçalves
327 Ferreira et al. 2013). It has been hypothesized that the free electrons can reduce multivalent
328 transition metals while reduced ions in the glass can potentially capture the positive hole centers
329 to transform to more oxidized species.

330 The XAFS spectral changes observed here in glasses with starting V^* greater than ~ 3.7 are
331 consistent with beam-induced reduction of V valence and is the dominant change observed in V
332 speciation due to irradiation. The pronounced decreases in pre-edge peak intensity, the shifting
333 of E_0 to lower energy and the changes observed in white line structure are all expected to occur
334 with V reduction (Lanzirotti et al. 2018). We hypothesize that V^{4+} and V^{5+} ions in these glasses
335 are able to capture available free electrons produced during irradiation to convert to V^{3+} and V^{4+}
336 ions, respectively. Such valence reductions are potentially accounted for by electron capture
337 reactions, consistent with what has been suggested from previous glass irradiation studies (El
338 Batal and Naf 2005; Abdelghany and ElBatal 2012). That the degree of beam-induced reduction
339 decreases with decreasing V^* , so that glasses with initial V^* value < 3.7 show only small
340 changes in V XAFS pre-edge peak intensity with increasing dose, imply that this is the point at
341 which the fraction of V^{3+} becomes significant and the effects of continued oxidation of V are
342 near the uncertainty level.

343 The possibility that some small degree of beam-induced oxidation of V^{3+} is occurring in the
344 most reduced glasses analyzed cannot be conclusively discounted. Studies have shown that

345 irradiation of synthetic silicate, borate and soda lime glasses may result in the potential oxidation
346 of reduced multivalent elements such as Fe^{2+} , Ce^{3+} , Cu^+ and Mn^{2+} (Bishay 1970; El Batal and
347 Naf 2005), hypothetically attributed to the reduced ions trapping holes via photochemical
348 reactions. However, any such oxidation in the glasses studied here is within analytical
349 uncertainty in fitting the pre-edge peaks. Oxidation of V^{3+} also appears to be inconsistent with
350 the measured decreases of the E_0 absorption edge in the V XAFS with increasing dose, by as
351 much as -0.8 eV for the most reduced glass analyzed here.

352 Even so, these more reduced glasses do display continued spectroscopic changes with
353 irradiation, even though not clearly associated with changes in valence. There are observed
354 increases in spectral intensity of the low energy shoulder at ~ 5475 eV, most likely reflecting
355 changes in vanadium-oxygen complexing and coordination within the glass network during
356 irradiation. Such effects can elevate the spectral backgrounds on the rising absorption edge and
357 may account for the small increases measured in instantaneous count rate near the pre-edge peak
358 with increasing dose. These changes in speciation seem to occur in all the glasses analyzed,
359 regardless of valence.

360 **IMPLICATIONS**

361 Although V K-edge XAFS is highly sensitive to detecting small variations in V valence due
362 to changing magmatic redox conditions, beam-induced changes in V speciation are likely to
363 introduce systematic errors in calculated V^* estimates, particularly in oxidized systems, that
364 must be properly evaluated and/or mitigated in order to make meaningful interpretations with
365 regards to the igneous evolution of the system.

366 The study presented here demonstrates that there are clear changes in V speciation that can
367 occur during XAFS analysis of silicate glasses and that the magnitude of the observed beam-

368 induced modifications is dependent on both the radiation dose over the period of analysis and the
369 starting valence of the samples being analyzed. The highest observed changes in valence
370 occurred at flux densities $> 6 \times 10^{11}$ ph/s/ μm^2 , resulting in reductions in calculated V^* on the
371 order of 0.3 valence units for the most oxidized glasses analyzed ($V^* = 4.94$). A difference in
372 assumed V^* of 0.3 valence units can translate to differences in calculated $f\text{O}_2$ of as much as ~ 0.5
373 log units for terrestrial magmatic glasses equilibrated at ~ 1200 °C (Sutton et al. 2005),
374 depending on redox conditions at equilibration, illustrating the importance of identifying the
375 potential for such alterations to occur at the time of analysis. However, for the majority of
376 terrestrial basaltic melts where V^* is expected to be < 4 , the impact on calculated oxygen
377 fugacity will be significantly smaller.

378 Our low flux density data show that the radiation alteration effects can be mitigated by doing
379 the measurements under these conditions. At the lower flux densities that we tested, $\leq 1 \times 10^9$
380 ph/s/ μm^2 , measured changes in V^* were found to be < 0.04 for repeated analyses in a series,
381 typically within the analytical uncertainty in calculating V^* for any individual spectra using the
382 Sutton et al. (2005) calibration. It was also found that magmatic glasses with V^* values near 3.7
383 show the smallest degree of change in speciation, and thus calculated V^* , with dose. This is an
384 average V valence that is generally similar to that often measured for terrestrial basaltic glasses.
385 For example, the terrestrial basaltic glasses analyzed in Sutton et al. (2005) and Lanzirrotti et al.
386 (2018), equilibrated at $f\text{O}_2$ from NNO-1.6 and NNO-0.5, provide V^* values between 3.7 and 4.1.

387 These results allow us to infer negligible impact of potential radiation-induced effects on
388 previously published results, studies which didn't account for possible beam-induced changes in
389 V valence. For the glasses analyzed as part of the Sutton et al. (2005), we estimate that the
390 beamline configuration used for the majority of their analyses, with a roughly 4×4 μm focused

391 beam, would have been conducted using a flux density of $< 2 \times 10^9$ ph/s/ μm^2 . At this flux density
392 the most oxidized glasses analyzed may be expected to experience reductions in V^* of < 0.05 ,
393 within the quoted uncertainty of the analyses used to build their calibration curve. A study by
394 Righter et al. (2006) examining the oxidation state of vanadium in coexisting spinel and basaltic
395 melt reports V K-edge XAFS data collected at the same beamline at roughly the same time. The
396 three standard spinels presented in the Righter et al. (2006) study, which are expected to be fairly
397 resistant to beam-induced changes in speciation, are shown to lie very close to the Sutton 2005
398 calibration curve. Consistent with the hypothesis that at the flux density conditions used in the
399 Sutton 2005 study, beam-induced reduction in the glass data was likely negligible. The study by
400 Lanzirotti et al. (2018) developed V oxybarometry calibration models using multivariate analysis
401 to predict the fO_2 of equilibration in glasses of basaltic composition and then tested the models
402 on a suite of natural basaltic glasses. Recognizing the potential for beam-induced changes in V
403 valence, the XAFS data collected on reference glasses for this study used a defocused beam of
404 $30 \times 30 \mu\text{m}$ and purposely reduced incident flux, so that flux densities to the standards was
405 estimated to be $\sim 1 \times 10^8$ ph/s/ μm^2 , so that changes outside of analytical uncertainty are not
406 expected. Some of the analysis of natural glasses in this study did use a focused beam of $\sim 2 \times 2$
407 μm , which would increase flux density to $\sim 2 \times 10^{10}$ ph/s/ μm^2 . The natural glasses analyzed in that
408 study, however, yield V^* close to 4.1, so that beam reduction effects would be expected to
409 reduce pre-edge peak intensities by $< 5\%$. A study by Head et al. (2018) included some V XAFS
410 analyses of magmatic melt inclusions from Nyamuragira volcano, Africa using stated flux
411 density of $\sim 2.5 \times 10^{10}$ ph/s/ μm^2 , with calculated V^* values between ~ 3.1 and 3.8. Although some
412 reduction in V^* would be expected at these flux densities, given calculated V^* are < 4 it would
413 be expected to reduce pre-edge peak intensities by $< 5\%$.

414 The results presented here provide researchers a framework for conducting V K-edge XAFS
415 oxybarometry studies of natural magmatic glasses that will yield the most accurate estimate of
416 the fO_2 at which the magma quenched. For most terrestrial magmatic glasses, where V* is found
417 to be near 4, beam induced changes in valence can be effectively minimized to be within
418 analytical uncertainty of the XAFS analysis if incident flux densities are kept at $\leq 1 \times 10^9$
419 ph/s/ μm^2 . These results illustrate the importance of documenting not only the focused spot size
420 used in V XAFS analysis of silicate glasses but the incident flux as well, so that the flux density
421 can be estimated. This is a recommendation that has also been made for all XAFS analyses of
422 magmatic melt inclusions (Rose-Koga et al. 2021).

423 The results of this study also have potential implications for the irradiation behavior of other
424 multivalent trace elements in silicate glasses during XAFS analysis. Potential valence proxies for
425 fO_2 in igneous systems include several multivalent elements that can be measured using XAFS.
426 These are summarized in a review by Papike and coworkers (Papike et al. 2005, 2016) and
427 include elements such S, Ti, Mn, Cr, Eu, and Fe in addition to V. With the increasing availability
428 of brighter synchrotron sources and improved focusing optics capable of providing sub-
429 micrometer focused X-ray beams for spectroscopic analysis (and thus potentially higher flux
430 densities), it is important for researchers to accurately evaluate potential beam-induced changes
431 in valence state and speciation for the elements being measured in each geochemical system,
432 whether targets are magmatic silicate glasses or minerals.

433 ACKNOWLEDGEMENTS

434 This research was supported by National Science Foundation – Earth Sciences grants EAR-
435 1834930 and EAR- 1634415 and the Remote, In Situ, and Synchrotron Studies for Science and
436 Exploration 2 (RISE2) node of the NASA SSERVI program. XANES spectroscopy data were

437 collected at GeoSoilEnviroCARS (Sector 13), Advanced Photon Source (APS), Argonne
438 National Laboratory. GeoSoilEnviroCARS is supported by the National Science Foundation,
439 Earth Sciences (EAR – 1634415). Use of the Advanced Photon Source was supported by the
440 U.S. Department of Energy, Office of Science, Office of Basic Energy Sciences, under contract
441 no. DE-AC02-06CH11357. We acknowledge the Smithsonian Institute National Museum of
442 Natural History Department of Mineral Sciences for providing samples of basaltic glass
443 standards VG-2 (NMNH 111240-52) and A-99 (NMNH 113498-1). We also want to
444 acknowledge Ben Hanson and John H. Jones for producing synthetic glasses used in this study
445 and making them available. We thank Kevin Righter and Bjorn von der Heyden for helpful and
446 constructive reviews of the manuscript and Sasa Bajt for editorial handling.

447 **REFERENCES CITED**

- 448 Abdelghany, A., and ElBatal, H. (2012) Structural evaluation and shielding behavior of gamma irradiated
449 vanadium doped silicophosphate glasses. *Journal of Molecular Structure*, 1024, 47–53.
- 450 Ballhaus, C., Berry, R.F., and Green, D.H. (1990) Oxygen fugacity controls in the Earth's upper mantle.
451 *Nature*, 348, 437–440.
- 452 Bishay, A. (1970) Radiation induced color centers in multicomponent glasses. *Journal of Non-Crystalline*
453 *Solids*, 3, 54–114.
- 454 Bunker, G. (2010) *Introduction to XAFS: a practical guide to X-ray absorption fine structure*
455 *spectroscopy*. Cambridge University Press.
- 456 Camara, B., and Oel, H.J. (1984) Behaviour and effect of iron in X-ray irradiated silicate glass. *Journal of*
457 *non-crystalline solids*, 65, 161–176.
- 458 Carmichael, I.S.E. (1991) The redox states of basic and silicic magmas: a reflection of their source
459 regions? *Contributions to Mineralogy and Petrology*, 106, 129–141.
- 460 Christie, D.M., Carmichael, I.S., and Langmuir, C.H. (1986) Oxidation states of mid-ocean ridge basalt
461 glasses. *Earth and Planetary Science Letters*, 79, 397–411.
- 462 Cottrell, E., Kelley, K.A., Lanzirotti, A., and Fischer, R.A. (2009) High-precision determination of iron
463 oxidation state in silicate glasses using XANES. *Chemical Geology*, 268, 167–179.
- 464 Cottrell, E., Lanzirotti, A., Mysen, B., Birner, S., Kelley, K.A., Botcharnikov, R., Davis, F.A., and
465 Newville, M. (2018) A Mössbauer-based XANES calibration for hydrous basalt glasses reveals

- 466 radiation-induced oxidation of Fe. *American Mineralogist: Journal of Earth and Planetary*
467 *Materials*, 103, 489–501.
- 468 El Batal, F.H., and Naf, S.M.A. (2005) Spectroscopic studies of gamma-irradiated transition metals-
469 doped soda lime phosphate glass.
- 470 Gaborieau, M., Laubier, M., Bolfan-Casanova, N., McCammon, C.A., Vantelon, D., Chumakov, A.I.,
471 Schiavi, F., Neuville, D.R., and Venugopal, S. (2020) Determination of Fe³⁺/ΣFe of olivine-
472 hosted melt inclusions using Mössbauer and XANES spectroscopy. *Chemical Geology*, 547,
473 119646.
- 474 Giuli, G., Paris, E., Mungall, J., Romano, C., and Dingwell, D. (2004) V oxidation state and coordination
475 number in silicate glasses by XAS. *American Mineralogist*, 89, 1640–1646.
- 476 Gonçalves Ferreira, P., de Ligny, D., Lazzari, O., Jean, A., Gonzalez, O.C., and Neuville, D. (2013)
477 Photoreduction of iron by a synchrotron X-ray beam in low iron content soda-lime silicate
478 glasses. *Chemical Geology*, 346, 106–112.
- 479 Hanson, B., and Jones, J.H. (1998) The systematics of Cr³⁺ and Cr²⁺ partitioning between olivine and
480 liquid in the presence of spinel. *American Mineralogist*, 83, 669–684.
- 481 Head, E., Lanzirrotti, A., Newville, M., and Sutton, S. (2018) Vanadium, Sulfur, and Iron Valences in
482 Melt Inclusions as a Window into Magmatic Processes: A Case Study at Nyamuragira Volcano,
483 Africa. *Geochimica et Cosmochimica Acta*, 226, 149-173.
- 484 Henderson, G.S., De Groot, F.M., and Moulton, B.J. (2014) X-ray absorption near-edge structure
485 (XANES) spectroscopy. *Reviews in Mineralogy and Geochemistry*, 78, 75–138.
- 486 Huebner, J.S., and Sato, M. (1970) The oxygen fugacity-temperature relationships of manganese oxide
487 and nickel oxide buffers. *American Mineralogist*, 55, 934–952.
- 488 Jarosewich, E., Nelen, J. a., and Norberg, J.A. (1980) Reference Samples for Electron Microprobe
489 Analysis. *Geostandards Newsletter*, 4, 43–47.
- 490 Jugo, P.J., Wilke, M., and Botcharnikov, R.E. (2010) Sulfur K-edge XANES analysis of natural and
491 synthetic basaltic glasses: Implications for S speciation and S content as function of oxygen
492 fugacity. *Geochimica et Cosmochimica Acta*, 74, 5926–5938.
- 493 Karner, J.M., Sutton, S.R., Papike, J.J., Shearer, C.K., Jones, J.H., and Newville, M. (2006) Application
494 of a new vanadium valence oxybarometer to basaltic glasses from the Earth, Moon, and Mars.
495 *American Mineralogist*, 91, 270–277.
- 496 Kelley, K.A., and Cottrell, E. (2009) Water and the oxidation state of subduction zone magmas. *Science*,
497 325, 605–607.
- 498 Klimm, K., Kohn, S.C., O’Dell, L.A., Botcharnikov, R.E., and Smith, M.E. (2012) The dissolution
499 mechanism of sulphur in hydrous silicate melts. I: Assessment of analytical techniques in
500 determining the sulphur speciation in iron-free to iron-poor glasses. *Chemical Geology*, 322–323,
501 237–249.
- 502 Knoll, G.F. (2010) *Radiation detection and measurement*. John Wiley & Sons.

- 503 Kraft, S., Stümpel, J., Becker, P., and Kuetsgens, U. (1996) High resolution x-ray absorption spectroscopy
504 with absolute energy calibration for the determination of absorption edge energies. *Review of*
505 *Scientific Instruments*, 67, 681–687.
- 506 Lanzirotti, A., Newville, M., Manoukian, L., and Lange, K. (2016) High-speed, coupled micro-beam
507 XRD/XRF/XAFS mapping at GSECARS: APS beamline 13-ID-E. In *Clay Mineral Society*
508 *Workshop Lecture Series: Filling the Gaps - From Microscopic Pore Structures to Transport*
509 *Properties in Shales Vol. 21*, pp. 53–64. Clay Mineral Society.
- 510 Lanzirotti, A., Dyar, M.D., Sutton, S., Newville, M., Head, E., Carey, C., McCanta, M., Lee, L., King,
511 P.L., and Jones, J. (2018) Accurate predictions of microscale oxygen barometry in basaltic
512 glasses using V K-edge X-ray absorption spectroscopy: A multivariate approach. *American*
513 *Mineralogist*, 103, 1282–1297.
- 514 Mathez, E.A. (1984) Influence of degassing on oxidation states of basaltic magmas. *Nature*, 310, 371–
515 375.
- 516 Moussallam, Y., Longpré, M.-A., McCammon, C., Gomez-Ulla, A., Rose-Koga, E.F., Scaillet, B., Peters,
517 N., Gennaro, E., Paris, R., and Oppenheimer, C. (2019) Mantle plumes are oxidised. *Earth and*
518 *Planetary Science Letters*, 527, 115798.
- 519 Nakada, R., Usui, T., Ushioda, M., and Takahashi, Y. (2020) Vanadium micro-XANES determination of
520 oxygen fugacity in olivine-hosted glass inclusion and groundmass glasses of martian primitive
521 shergottite Yamato 980459. *American Mineralogist*, 105, 1695–1703.
- 522 Papike, J.J., Karner, J.M., and Shearer, C.K. (2005) Comparative planetary mineralogy: Valence state
523 partitioning of Cr, Fe, Ti, and V among crystallographic sites in olivine, pyroxene, and spinel
524 from planetary basalts. *American Mineralogist*, 90, 277–290.
- 525 Papike, J.J., Simon, S.B., Burger, P.V., Bell, A.S., Shearer, C.K., and Karner, J.M. (2016) Chromium,
526 vanadium, and titanium valence systematics in Solar System pyroxene as a recorder of oxygen
527 fugacity, planetary provenance, and processes. *American Mineralogist*, 101, 907–918.
- 528 Righter, K., Sutton, S., Newville, M., Le, L., Schwandt, C., Uchida, H., Lavina, B., and Downs, R.T.
529 (2006) An experimental study of the oxidation state of vanadium in spinel and basaltic melt with
530 implications for the origin of planetary basalt. *American Mineralogist*, 91, 1643–1656.
- 531 Rose-Koga, E.F., Bouvier, A.-S., Gaetani, G.A., Wallace, P.J., Allison, C.M., Andrys, J.A., de la Torre
532 CA, A., Barth, A., Bodnar, R.J., Ajj, B.G., and others (2021) Silicate melt inclusions in the new
533 millennium: A review of recommended practices for preparation, analysis, and data presentation.
534 *Chemical Geology*, 120145.
- 535 Rowe, M.C., Kent, A.J., and Nielsen, R.L. (2007) Determination of sulfur speciation and oxidation state
536 of olivine hosted melt inclusions. *Chemical Geology*, 236, 303–322.
- 537 Sato, M. (1978) Oxygen fugacity of basaltic magmas and the role of gas-forming elements. *Geophysical*
538 *Research Letters*, 5, 447–449.
- 539 Sutton, S., Lanzirotti, A., Newville, M., Dyar, M.D., and Delaney, J. (2020) Oxybarometry and valence
540 quantification based on microscale X-ray absorption fine structure (XAFS) spectroscopy of
541 multivalent elements. *Chemical Geology*, 531, 119305.

- 542 Sutton, S.R., Karner, J., Papike, J., Delaney, J.S., Shearer, C., Newville, M., Eng, P., Rivers, M., and
543 Dyar, M.D. (2005) Vanadium K edge XANES of synthetic and natural basaltic glasses and
544 application to microscale oxygen barometry. *Geochimica et Cosmochimica Acta*, 69, 2333–2348.
- 545 Sutton, S.R., Lanzirotti, A., Newville, M., Rivers, M.L., Eng, P., and Leticariu, L. (2017) Spatially
546 Resolved Elemental Analysis, Spectroscopy and Diffraction at the GSECARS Sector at the
547 Advanced Photon Source. *Journal of Environmental Quality*, 46, 1158–1165.
- 548 Trail, D., Tailby, N.D., Lanzirotti, A., Newville, M., Thomas, J.B., and Watson, E.B. (2015) Redox
549 evolution of silicic magmas: Insights from XANES measurements of Ce valence in Bishop Tuff
550 zircons. *Chemical Geology*, 402, 77–88.
- 551 Wilke, M., Jugo, P.J., Klimm, K., Susini, J., Botcharnikov, R., Kohn, S.C., and Janousch, M. (2008) The
552 origin of S⁴⁺ detected in silicate glasses by XANES. *American Mineralogist*, 93, 235–240.
- 553 Wong, J., Lytle, F.W., Messmer, R.P., and Maylotte, D.H. (1984) K-edge absorption spectra of selected
554 vanadium compounds. *Physical Review B*, 30, 5596.
- 555 Zhang, J., Dong, W., Qiao, L., Li, J., Zheng, J., and Sheng, J. (2007) Silver nanocluster formation in soda-
556 lime silicate glass by X-ray irradiation and annealing. *Journal of crystal growth*, 305, 278–284.

557

558

FIGURE CAPTIONS

559 Figure 1: Measured edge-step normalized V K-edge XAFS spectra collected for FAD_V3, the
560 most oxidized glass analyzed (top), and FAD_V2a, the most reduced glass analyzed (bottom),
561 measured at flux densities of 2.56×10^8 (in red) and 9.25×10^{11} (in blue) $\text{ph/s}/\mu\text{m}^2$. The inset plots
562 on each show the relative magnitude of the measured pre-edge peaks for both glasses after
563 subtracting the edge step contribution via spline fitting of the rising absorption edge. Although
564 the background subtracted spectra for oxidized glass FAD_V3 indicate an ~30% reduction in
565 pre-edge peak intensity after subtraction of the spectral background, the background subtracted
566 peak intensities for reduced glass FAD_V2a displays a <1% difference at the two flux densities
567 tested. Glass FAD_V3 also displays a decrease in the energy of the main absorption edge (E_0) of
568 1.1 eV with increasing radiation dose. Glass FAD_V2a displays a decrease of 0.8 eV in E_0 with
569 increasing dose. The dashed line shows a low energy shoulder at ~ 5475 eV on the rising

570 absorption edge that increases in intensity with increasing dose in both samples. This increasing
571 shoulder in FAD_V2a may be responsible for the increasing background under the pre-edge peak
572 and the decrease in E_0 .

573 Figure 2: Series of rapid V K-edge XAFS spectra collected on reduced synthetic glasses
574 FAD_V2a (top) and FAD_V4 (bottom) conducted at a low density of 7.75×10^8 ph/s/ μm^2 (left)
575 and a high flux density of 6.25×10^{11} ph/s/ μm^2 (right). Shown are a series of 10 edge-step
576 normalized V K-edge XAFS spectra that were measured sequentially, with each scan acquired in
577 ~ 1.5 minutes. Acquisition of 10 total spectra requires the glass to undergo irradiation at each flux
578 density for a total time of ~ 15 minutes. The inset plots on each figure show the pre-edge peak
579 portion of each scan and provide calculated V^* for each scan using the Sutton et al. (2005)
580 calibration, which subtracts the pre-edge background.

581
582 Figure 3: Series of rapid V K-edge XAFS spectra collected on oxidized synthetic glasses
583 FAD_V1a (top) and FAD_V3 (bottom) conducted at a low and high flux density as described in
584 Fig. 2.

585
586 Figure 4: Series of rapid V K-edge XAFS spectra collected on natural MORB glass VG-2 at a
587 low and high flux density as described in Fig. 2.

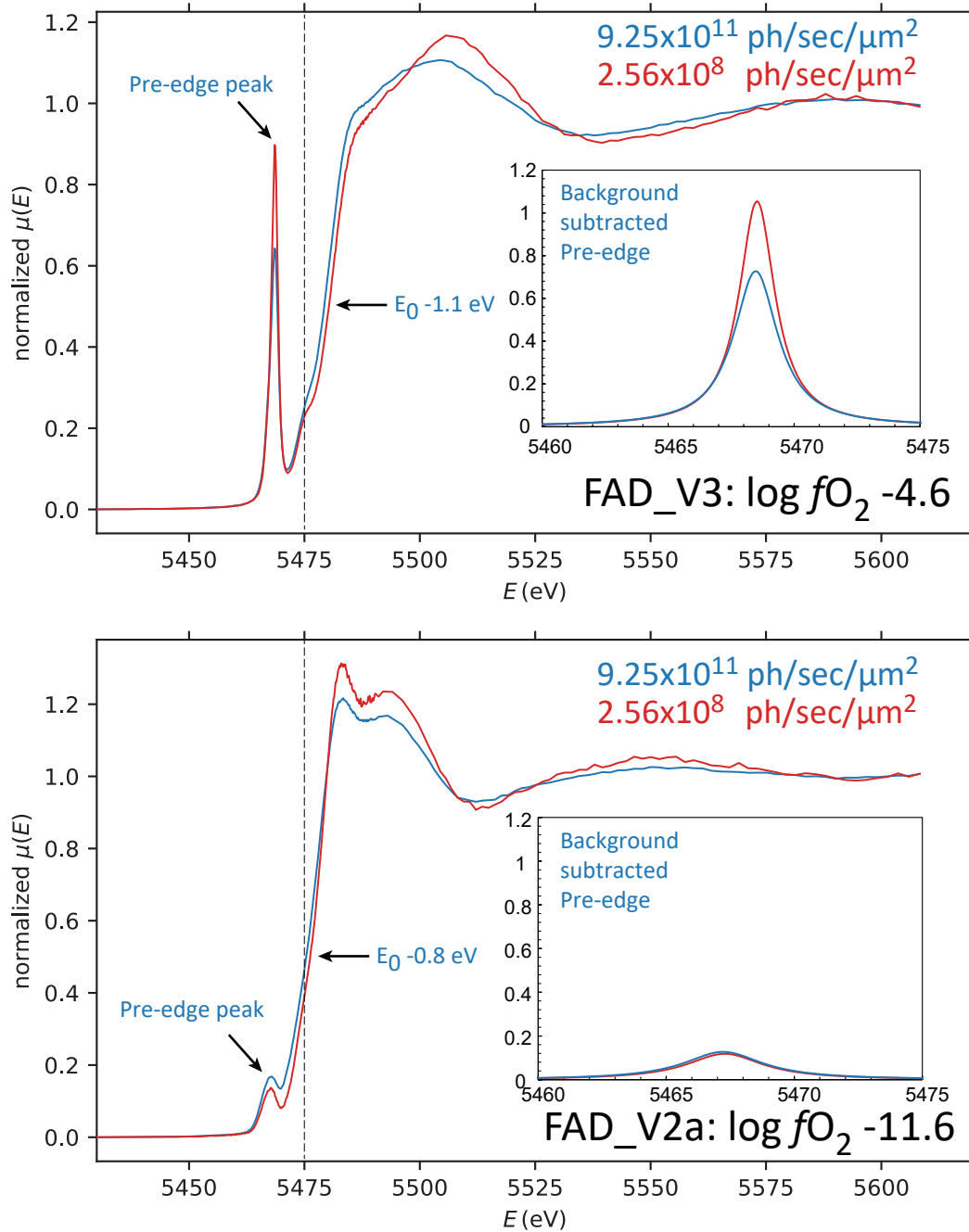
588
589 Figure 5: Plots of the relative calculated V^* for the rapid synthetic glass XAFS analyses
590 FAD_V2a (blue), FAD_V4 (red), FAD_V1a (gray) and FAD_V3 (green) shown in Fig. 2 and 3
591 as a function of time. Calculated V^* from the low flux density series are shown as open squares

592 and from the high flux density series as filled circles. Error bars show estimated 1σ uncertainties
593 in calculating V^* .

594

595 Figure 6: V pre-edge intensity rate-of-change curves for oxidized FAD_V1a, and FAD_V3 and
596 for natural basaltic glasses VG-2 and A-99, collected at varying flux densities. Flux densities
597 tested are labeled, covering more than 4 orders of magnitude. Intensities were measured at the V
598 pre-edge peak at an energy of 5468.15 eV. Each time series consists of measurements at 1s
599 intervals over 1500s of total irradiation. The vertical axis shows the relative change in the pre-
600 edge peak intensity over time, so that for each curve the intensity of the first analysis point plots
601 at a value of 1.0.

Figure 1



Most Reduced

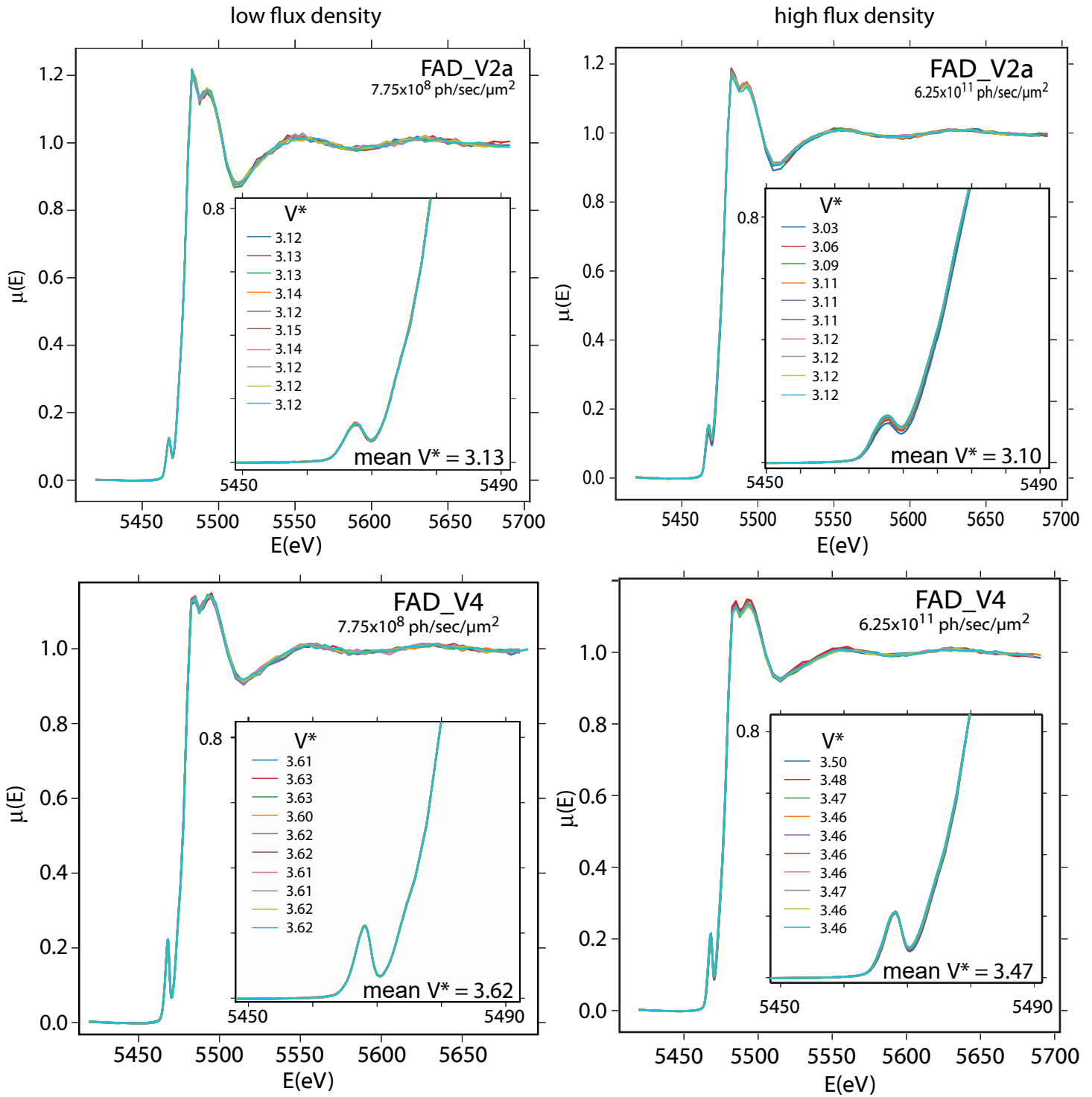


Figure 2

Figure 3

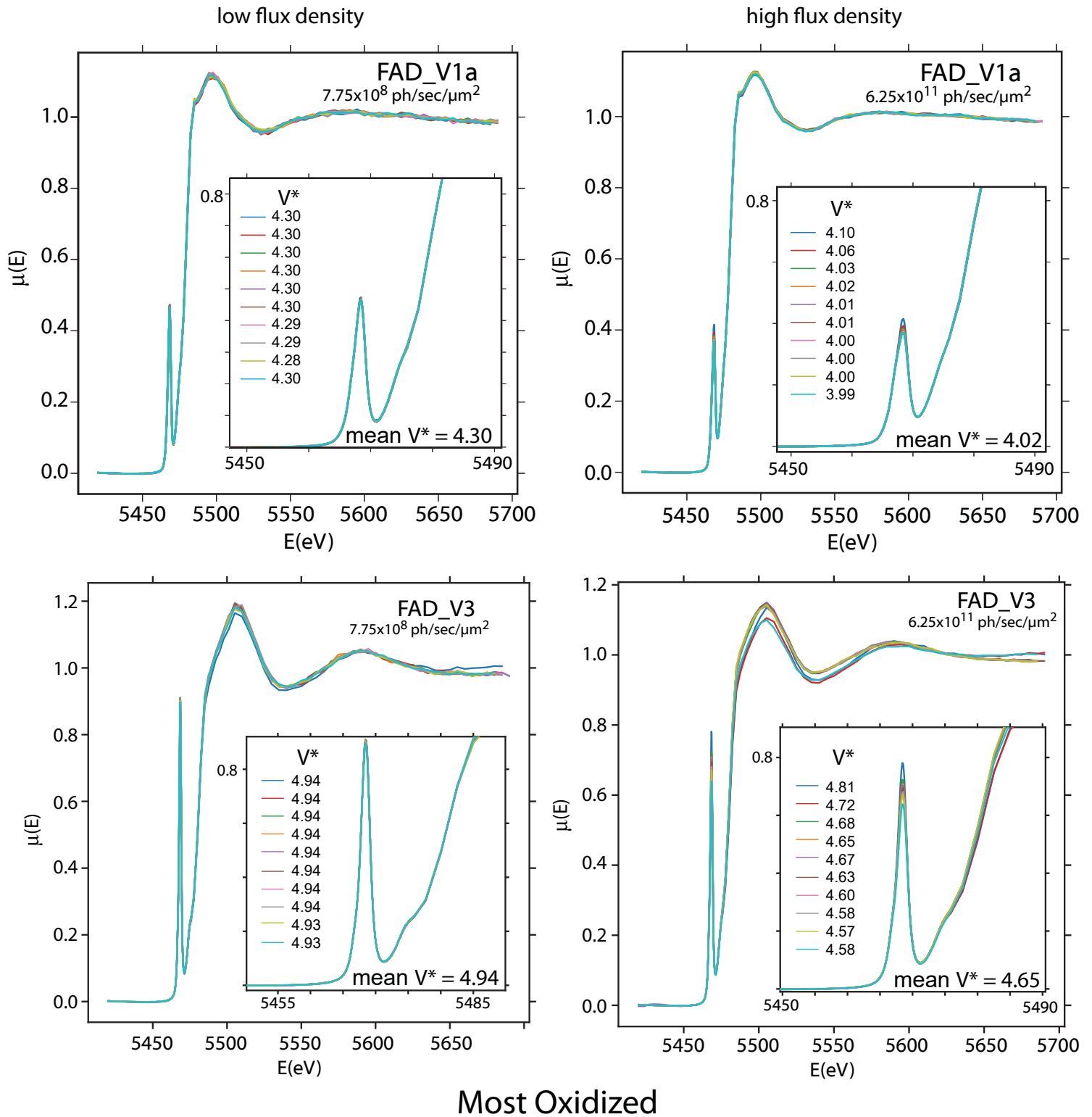


Figure 4

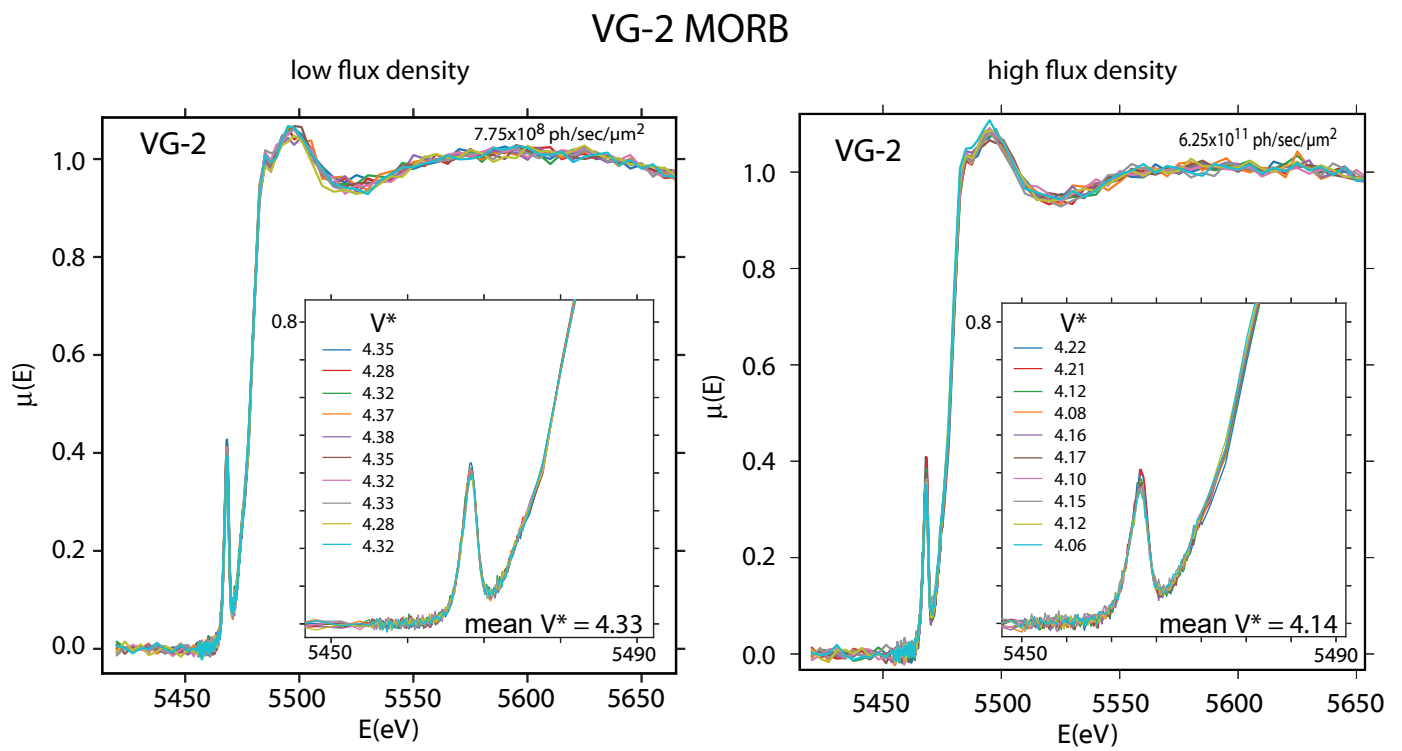


Figure 5

